Crosstalk between Nitric Oxide and Retinoic Acid pathways is essential for amphioxus pharynx development

Caccavale F[1], Annona G[1], Subirana L[2], Escriva H[2], Bertrand S[2], D'Aniello S[1,*]

[1] Department of Biology and Evolution of Marine Organisms (BEOM), Stazione Zoologica Anton Dohrn Napoli, Napoli, Italy.

[2] Sorbonne Université, CNRS, Biologie Intégrative des Organismes Marins (BIOM), Observatoire Océanologique, Banyuls-sur-Mer, France.

* Salvatore D'Aniello < salvatore.daniello@szn.it>

ORCID: 0000-0001-7294-1465

Abstract

During animal ontogenesis, body axis patterning is finely regulated by complex interactions between several signaling pathways. Nitric Oxide (NO) and Retinoic Acid (RA) are potent morphogens that play a pivotal role in vertebrate development. Their involvement in axial patterning of head and pharynx shows conserved features in the chordate phylum. Indeed, in the cephalochordate amphioxus NO and RA are crucial for the correct development of pharyngeal structures. Here we demonstrate the functional cooperation between NO and RA occurring in amphioxus embryogenesis. During neurulation, NO modulates RA production through the transcriptional regulation of Aldh1a.2 that irreversibly converts retinaldehyde into RA. On the other hand, RA regulates the transcription of Nos genes, probably through RA Response Elements found in their regulatory regions. The reciprocal regulation of NO and RA

pathways results to be essential for the normal pharyngeal development in amphioxus and suggests that this regulatory crosstalk could be conserved in vertebrates.

Keywords

Nitric Oxide Synthase; RA pathway; Chordate; Developmental Biology; Evolution.

Introduction

The ontogenesis of the vertebrate head is a complex developmental process in which both neural crest and non-neural crest cells participate. The craniofacial development and the correct antero-posterior patterning of head structures are driven by complex interactions between several signaling pathways and epigenetic mechanisms (Haworth et al., 2007; Jacox et al., 2014; Kong et al., 2014; Francis-West and Crespo-Enriquez, 2016). In this context Nitric Oxide (NO) is a potent morphogen playing crucial roles in head structures development. Loss-of-function of neuronal Nitric Oxide Synthase (*Nos1*) in *Xenopus* and zebrafish induces the arrest of mouth opening, smaller eye and strong aberrations in cartilage and bone structures formation (Jacox et al., 2014). Moreover, the inhibition of NO production is responsible for severe defects in pharyngeal arches patterning, consistent with alterations in the Hox code (Kong et al., 2014).

The development and the antero-posterior and dorso-ventral patterning of the head and pharynx show conserved features within the chordate phylum. In amphioxus, which belongs to the cephalochordate subphylum, pharynx is characterized by a marked left-right asymmetry which is controlled by the Nodal signaling pathway, namely by the Cerberus-Nodal-Lefty-Pitx

cascade (Bertrand et al., 2015; Soukup et al., 2015; Li et al., 2017). The antero-posterior patterning and development of amphioxus pharyngeal slits are driven by a conserved set of transcription factor genes, among which *Hox1, Pax2/5/8, Pitx, Tbx1/10,* and *Engrailed* (Schubert et al., 2005; Bertrand et al., 2015; Wang et al., 2019) similarly to the development of pharyngeal arches in vertebrates.

NO is enzymatically produced in amphioxus by three distinct NO synthase genes: *NosA, NosB* and *NosC,* derived from cephalochordate-specific gene duplications and showing a complementary expression pattern during development (Annona et al., 2017). During amphioxus embryonic development, as a consequence of pharmacological inhibition of endogenous NO production, the opening of the mouth is prevented as well as the correct development of other important pharyngeal structures, such as the endostyle and the club-shaped gland (Annona et al., 2017). Moreover, the larvae show a posteriorized phenotype, resembling the well described phenotype induced by RA administration during amphioxus embryogenesis (Escriva et al., 2002; Schubert et al., 2005; Koop et al., 2014). These experimental evidences prompted us to investigate the hypothesis of a possible evolutionarily conserved role of NO and RA in chordate pharynx development using the cephalochordate *Branchiostoma lanceolatum* as a model system. In order to highlight the molecular mechanisms driving developmental changes in the amphioxus embryo, we took advantage of the transcriptomic differences induced by pharmacological treatments reducing endogenous NO production, which alter the pharyngeal area development (Annona et al., 2017). Our approach allowed us to demonstrate that such morphogenetic alterations are linked to a dramatic imbalance affecting the reciprocal regulation of NO and RA pathways.

Results

NO controls pharyngeal development during early neurulation in amphioxus

Previous studies have highlighted the involvement of NO in the specification of amphioxus pharyngeal structures (Annona et al., 2017). To better characterize the key role of NO during embryonic development, we decided to narrow down the time window of treatment by defining the exact timing during which NO is functional. Therefore, we performed short-term *in vivo* treatments with the NOS activity inhibitor 1-[2-(trifluoromethyl)phenyl]-1H-imidazole (TRIM) during *B. lanceolatum* development using different drug exposure times between early neurula stage (N2 stage) and pre-mouth larva stage (transition stage T2) (Figure 1A). The resulting phenotype was then observed at the open-mouth larva stage (larva-L0 stage). The observed morphological alterations included: *i.* a reduced antero-posterior length of the pharynx, *ii.* a complete or partial absence of mouth opening on the left side of the pharynx (Figure 1B, section c and c'), *iii.* an incomplete formation of the club-shaped gland and of the endostyle (Figure 1B, section d, e and d', e'), and *iv.* a smaller first gill slit (Figure 1B, section f and f').

The inhibition of NO production during the time window 24-30 hours post fertilization (hpf, at 18°C) was the shortest treatment inducing a strong effect by producing 100% of abnormal larval while delayed treatments starting at 30 or 36 hpf, for 6, 12 or 24 hours, resulted in approximately 70% of affected larvae. Conversely, when TRIM treatment was performed later, between 42 and 48 hpf, the larvae were not affected (Figure 1A). These results suggest, therefore, that pharyngeal development is, at least in part, under the control of NO during neurulation and that the critical time of its action is restricted approximately to six hours. Based on these experimental evidences, we performed a differential transcriptomic analysis comparing TRIM-treated embryos (continuous treatment from 24 to 30 hpf) with wild-type

99 embryos in order to define the genes acting downstream of NO signaling during pharyngeal
100 development in amphioxus (Figure. 1C - figure supplement 1).
101
102 **Inhibition of NO synthesis *in vivo* induces up-regulation and ectopic expression of RA**
103 **pathway genes**
104 The differential RNA-Seq analysis of TRIM-treated embryos (30 hpf) revealed the up-regulation
105 of 392 and the down-regulation of 50 genes (Figure 1 C - figure supplement 1 panels A-B-C).
106 Interestingly, several differentially up-regulated genes are implicated in RA metabolism and
107 signaling pathway (synthesis and storage, catabolism, and known direct RA target genes):
108 *Adh3, Rdh11/12.18, Aldh1a.2, Crabp, Cyp26.1, Cyp26.2, Cyp26.3, RAR, Hox1, Hox3, Meis*
109 (Figure 1C – figure supplement 2). In order to confirm this finding, the expression levels of
110 several of these genes were additionally analyzed by quantitative RT-PCR (qRT-PCR). The
111 results showed a consistent expression change trend with the RNA-seq data (Figure 1C - figure
112 supplement 1 panel D). Moreover, the expression pattern of RA target genes *Hox1*, *Hox3*, *Meis*
113 and *Cyp26* genes was further investigated by whole-mount *in situ* hybridization in both control
114 and TRIM-treated embryos at the neurula N4 and pre-mouth T2 developmental stages. Such
115 analyses showed that endogenous NO reduction produced an effect not only on the expression
116 level of RA metabolism and signaling pathway genes, but also on the expression territories of
117 most of them. *Hox1, Hox3* and *Meis* anterior limit of expression was pushed anteriorly in TRIM-
118 treated embryos in comparison to controls, indicative of the embryo posteriorization (Figure
119 2A). The RA catabolism genes that are duplicated in amphioxus, *Cyp26.1, Cyp26.2, Cyp26.3*,
120 denoted an heterogeneous behavior: *Cyp26.2* was slightly up-regulated and its expression
121 pattern did not change after TRIM treatment, whereas *Cyp26.1* and *Cyp26.3* were strongly up-
122 regulated and showed an ectopic expression (Figure 2A). In particular, after inhibition of NO

production, *Cyp26.1* expression was anteriorized, while *Cyp26.3* expression was posteriorized. Moreover, *Cyp26.3* showed an additional domain of expression in the tailbud, mainly in the pre-mouth larvae (Figure 2A).

Aldh1a.2 is specifically regulated by NO

The above-mentioned gene expression results suggested that the abnormal pharyngeal development of TRIM-treated embryos could be the result of an up-regulation of the RA signaling pathway. In order to test this hypothesis, we performed two *in vivo* experiments in parallel in which early neurula embryos were incubated for 6 hours, from 24 to 30 hpf, in the presence of either TRIM or RA. Then, we analyzed the relative expression of three groups of genes, that previously we found to be up-regulated in our RNA-seq analysis, by qRT-PCR: *i.* genes involved in the synthesis and in storage of RA, as *Adh3*, *Rdh11/12*, *Aldh1a.2*, *Crabp*; *ii.* genes that mediate RA effects, as *RAR*, *Hox1*, *Hox3*, *Meis*; and *iii)* genes involved in RA degradation, as *Cyp26.1*, *Cyp26.2*, *Cyp26.3*. All analyzed genes were up-regulated after both TRIM and RA treatment, with the exception of *Aldh1a.2* which was exclusively up-regulated after TRIM treatment (Figure 2 B-C-D).

NosA and _NosB_ respond to exogenous RA during development

The expression analysis of the three amphioxus *Nos* genes after TRIM treatment revealed the transcriptional up-regulation for two of them, *NosA* and *NosB*, while *NosC*, the only one constitutively expressed during development (Annona et al., 2017) remained insensitive to the pharmacological treatment (Figure 2E).

In order to check if *NosA* and *NosB* up-regulation could be due to an indirect effect of the intracellular increase of RA caused by the TRIM treatment, we tested their expression levels

after the addition of exogenous RA (Figure 2E). Similarly, to the TRIM treatment, we observed that *NosA* and *NosB* expression were significantly up-regulated also as a consequence of RA administration. Moreover, exogenous RA induces up-regulation of *NosA* expression up to 36 hpf and *NosB* expression up to 48 hpf (Figure 2E - figure supplement 3 panel A).

These experimental evidences suggest a possible transcriptional effect of RA on *Nos* genes during embryogenesis in amphioxus. To further support this assumption, we searched for the presence of Retinoic Acid Response Elements (RARE) in the putative regulatory genomic regions of *NosA* and *NosB,* using a computational prediction tool. We looked for RAREs in selected open chromatin regions identified by the overlapping peaks obtained from ATAC-seq and Chip-seq data (Marlétaz et al., 2018). Six putative Direct Repeat (DR)-type binding sites were detected in the *NosA* locus (two DR1, three DR3 and one DR5), and only one DR5 in the 5' region of *NosB* (Figure supplement 3 panel B), suggesting a possible direct RA regulation of *Nos* genes in amphioxus.

A RALDH inhibitor and a RAR antagonist are able to rescue the normal phenotype after inhibition of NO synthesis

To confirm that the up-regulation of *Aldh1a.2*, which could result in an endogenous RA increase, is the key event underlying pharyngeal alterations in TRIM-treated larvae, we performed two independent phenotypic rescue experiments using the RALDH inhibitor DEAB (N,N-diethylaminobenzaldehyde) and the RA antagonist BMS009. Both DEAB and BMS009 were applied in combination with TRIM to embryos at 24 hpf and removed at 30 hpf. As a control, the TRIM treatment was performed in parallel on another batch of embryos. The combined treatment with TRIM and DEAB resulted in the recovery of the wild type phenotype in 76% of the total observed larvae, while 14% of them showed a partially recovered phenotype

with a smaller mouth compared to controls (Figure 3A, B). The rescue experiments performed using the combination of TRIM and BMS009 led to 54% of complete and 21% of partial recovery of the wild type larval morphology (Figure 3A). Moreover, these morphological rescue experiments were associated with the recovery at N4 neurula stage of the normal expression pattern of RA catabolism (*Cyp26.1* and *Cyp26.3*) and RA target (*Hox1*, *Hox3* and *Meis*) genes (Figure 3C).

Therefore, by using two independent experiments, we demonstrate that the reduction of RA levels, or of its regulatory action, in TRIM-treated embryos, rescues the wild type phenotype, suggesting that the observed phenotype in TRIM-treated embryos is produced by an increase in RA signaling.

Discussion

NO controls RA synthesis by the transcriptional regulation of *Aldh1a.2*

The inhibition of NO production during amphioxus neurulation affects the normal formation and localization of pharyngeal structures at the larva stage, including the length of the pharynx itself. From a molecular point of view, the differential RNA-seq approach revealed a clear up-regulation of different RA pathway players after Nos activity inhibition, suggesting that such de-regulation is responsible for the observed phenotype. The role of RA in pharyngeal morphogenesis has been extensively described in the literature; RA acts through *Hox1* in establishing the posterior limit of amphioxus pharynx. *Hox1* is co-expressed with the RA receptor (RAR) in the midgut endoderm and, in turn, represses the expression of pharyngeal endoderm markers, such as *Pax1/9* and *Otx* (Schubert et al., 2005). Nevertheless, the formation of pharyngeal slits requires low levels of RA. This condition is guaranteed *i.* by the activity of RA degradation enzymes (Cyp26), *ii.* by the expression of TR2/4, a transcriptional

repressor which binds on RAREs and decreases RA signaling in the anterior part of the animal, and *iii.* by the fact that the embryonic region producing RA (the central region of the embryo) moves posteriorly as the embryo elongates (Escriva et al., 2002; Koop et al., 2014). In our studies, as a result of Nos activity inhibition, the RA target genes, *Hox1*, *Hox3* and *Meis,* showed an increased expression level and an anterior limit of expression which is moved anteriorly, consistent with the posteriorization of the larva body plan. Furthermore, the RA degrading enzyme genes, *Cyp26.1* and *Cyp26.3*, were also sensible to the inhibition of endogenous NO production showing an increased and ectopic expression. *Cyp26* genes are required for RA degradation in endoderm and ectoderm and have a key role in the establishment and maintenance of the antero-posterior RA concentration gradient in amphioxus (Carvalho et al., 2017a). The up-regulation of Cyp26 genes is a known consequence of RA excess, which is responsible of the posteriorization of larval body structures and of the pharynx loss (Escriva et al., 2002; Schubert et al., 2005; Schubert et al., 2006; Minoux and Rijli, 2010 ; Koop et al., 2010, 2014; Bertrand et al., 2015; Carvalho et al., 2017b). Altogether, these results suggested that the observed phenotype in the TRIM-treated amphioxus embryos could be due to an increase in RA production. Intracellular RA is synthetized by the reversible oxidation of retinol in retinaldehyde by either alcohol dehydrogenases (ADH) or retinol dehydrogenases (RDH). Subsequently, retinaldehyde is irreversibly oxidized to RA by retinaldehyde dehydrogenases (RALDH), mainly by ALDH1A (Gallego et al., 2006; Duester, 2008). In particular, in our experiments we observed transcriptional up-regulation of *Adh3*, *Rdh11/12.18* and *Aldh1a.2* after TRIM treatments. The unique orthologue of vertebrate *Adh* genes, *Adh3*, was identified in amphioxus (Cañestro et al., 2002). Instead, 22 *Rdh11/12* genes in amphioxus, derived from a lineage-specific expansion, were identified as related to human *Rdh11*, *Rdh12, Rdh13* and *Rdh14,*

corresponding to retinaldehyde reductases predominantly involved in retinoid metabolism and homeostasis (Albalat et al., 2011) (Figure supplement 2). For *Aldh1*, a total of six genes were identified in amphioxus, orthologs of human *Aldh1A1-3,* which are major players in the oxidation of RA (Cañestro et al., 2006) (Figure supplement 2). In our study, *Adh3* and *Rdh11/12.18* genes also resulted up-regulated after administration of exogenous RA, suggesting a feedback regulation of RA synthesis by itself, at least on reversible enzymatic steps. On the other hand, *Aldh1a.2* was insensible to exogenous RA excess. Based on these results we hypothesized that, under physiological conditions, NO transcriptionally regulates *Aldh1a.2* and, as a consequence, controls the production of endogenous RA. Further evidence to support our hypothesis is provided by two independent rescue experiments. Technically, in association with TRIM, we used two drugs that specifically act on most crucial steps of RA signaling pathway: an inhibitor of the RALDH enzymes activity that would compensate the excess of Aldh1a.2, and a RA antagonist able to compensate the RA over-production through its binding to RAR. In both rescue experiments we observed not only the recovery of the wild type phenotype but also the restoration of the expression pattern of both RA-target and RA-degrading genes.

Therefore, based on our results, we propose NO as a key player in the fine regulation of RA synthesis during neurulation in amphioxus. Thus, NO fine-tune the expression of *Aldh1a.2*, keeping RA concentration within the optimal range. This precise balance between intracellular concentrations of NO and RA guarantees the correct expression levels and territory localization of all RA downstream target genes. When NO is removed from the system the RA metabolism machinery malfunctions, giving rise to a consequent cascade of events that lead to the up-regulation of the entire RA signaling pathway.

The missing piece of the puzzle, therefore, seems to be an unknown protein able to mediate the control of *Aldh1a.2* transcription by NO. The activity of such protein could depend on its phosphorylation and S-nitrosylation state that would be modulated by NO. Indeed, in other chordates, it has been demonstrated that the mechanisms by which NO regulates transcription of target genes are: *i.* the control of the extracellular-regulated kinase (ERK) and the MAP kinase phosphatases (MAPK) activity and, as a result, the modulation of phosphorylation or dephosphorylation of target transcription factors (Castellano et al., 2014), and *ii.* the direct modulation of target proteins, as transcription factors, histone acetyltransferases and deacetylases or DNA methyltranserases, through S-nitrosylation of specific cysteine residues (Bogdan, 2001; Nott et al., 2008; Sha and Marshall, 2012).

Hence, further research is necessary to find out which is the NO-target protein that mediates *Aldh1a.2* expression regulation and how NO specifically controls its activity. It could be important improve this knowledge since very little information, and only restricted to vertebrates, is reported on the control of RA metabolism by NO. Some cytochrome P450 enzymes, involved in RA–metabolism, were identified as putative NO–regulated proteins but no evidences about such a possible transcriptional regulation have been reported (Lee et al., 2014, 2017).

RA controls NO synthesis

The exogenous administration of RA induces the expression of two amphioxus *Nos* genes that are normally not expressed during development, *NosA* and *NosB* (Annona et al., 2017). Moreover, this activation is maintained throughout the whole critical time period during which NO is necessary for pharyngeal development (Figure supplement 3 panel A). Conversely,

265 *NosC*, the only *Nos* gene expressed during embryogenesis in normal conditions, seems not to
266 be affected by the increase of RA level.
267 The *in silico* analysis of the chromosomal loci of both *B. lanceolatum NosA* and *NosB* revealed
268 the presence of seven DR-type RAREs (Figure supplement 3 panel B), localized in open
269 chromatin regions detected by ATAC-seq and Chip-seq approaches. This suggests a possible
270 regulation of *Nos* genes by RA through the binding of RAR/RXR nuclear receptors to these
271 putative RAREs. The transcriptional activation of *NosA* and *NosB* by RA during development
272 could be part of a mechanism to rebalance the correct NO/RA ratio. However, this hypothesis
273 should be further confirmed by experimental validation.
274 In vertebrates, the role of NO and RA in the correct development of the pharynx and craniofacial
275 structures has already been described. For example, NO is described to be necessary for face
276 formation as part of the Kinin-Kallikrein pathway (Jacox et al., 2014) and, on the other hand,
277 the correct RA gradient, generated by local degradation, leads to appropriate specification of
278 craniofacial structures (Abe et al., 2008; Liu et al., 2013; Chawla et al., 2018).
279 However, a possible crosstalk between NO and RA pathways has not yet been revealed. As
280 mentioned above, there are few published data on the regulatory effect of NO on RA pathway,
281 while the control of RA on NO production in vertebrates is more documented. For instance, in
282 human cells, it has been demonstrated the inhibitory or activation effect of RA on NO production
283 through activation of inducible or endothelial NOS at both protein and transcript levels (Sirsjö
284 et al., 2000; Achan et al., 2002; Hattori et al., 2002; Behairi et al., 2015; Moon, 2019).
285

286 ## Conclusions

287 Our results show the presence of a functional crosstalk between RA and NO signals in the
288 cephalochordate amphioxus during neurulation. This opens new questions about the

289 evolutionary conservation of this regulatory loop in the development of the pharynx and the
290 head of vertebrates.
291 The role of RA as well as that of NO in amphioxus development and antero-posterior patterning
292 of the pharynx has been described in several studies. Our results suggest the occurrence of a
293 regulatory crosstalk between these two ancient and essential signaling pathways that has been
294 previously neglected. Based on our data we propose that, during amphioxus development, a
295 precise NO/RA balance is necessary for the correct antero-posterior patterning of the pharynx.
296 This endogenous intracellular balance is preserved by the reciprocal regulation of NO and RA
297 pathways. Given such evidences and knowledge from vertebrate literature, we hypothesize
298 that the functional and regulatory crosstalk between NO and RA pathways could be a
299 conserved feature in vertebrates.
300

301 ## Materials & Methods

302 ### Amphioxus embryos collection

303 Ripe adult European amphioxus (*Branchiostoma lanceolatum*) were collected in Argelès-sur-
304 mer (France) with a specific permission delivered by the Prefect of Region Provence Alpes
305 Côte d'Azur. *B. lanceolatum* is not a protected species. Spawning was induced during late
306 spring and beginning of summer by employing a thermal shock as described by Fuentes *et*
307 *al*.(Fuentes et al., 2007) After *in vitro* fertilization, embryos were cultured in 0,22 µm filtered
308 seawater at 18°C in plastic Petri dishes. Following the staging at 18°C, 24 hpf corresponds to
309 neurula 2 stage (N2), 30 hpf to neurula 4 stage (N4), 36 hpf to transition 1 stage (T1), 42 hpf
310 to transition 2 stage (T2), 48 hpf to transition 3 stage (T3), and 72 hpf to larva 0 (L0). At desired
311 developmental stages embryos were used for specific drug treatments, and then they were
312 frozen in liquid nitrogen and kept at -80°C for subsequent RNA extraction, or fixed with 4%

313 paraformaldehyde (PFA) in MOPS buffer overnight at 4°C and then stored in 70% ethanol at -
314 20°C.
315
316 **Pharmacological treatments**
317 Amphioxus embryos at different developmental stages were treated with the NOS inhibitor 1-
318 [2-(trifluoromethyl)phenyl]-1H-imidazole (TRIM), with the RALDH inhibitor N,N-
319 diethylaminobenzaldehyde (DEAB), with the RA antagonist BMS009 and with Retinoic Acid
320 (RA). All the drugs were dissolved in dimethyl sulfoxide (DMSO), and control embryo groups
321 for each treatment were prepared adding an equal amount of DMSO. For TRIM treatments, a
322 final concentration of 100 µM was used starting at 24 hpf. Embryos at 30, 36, 42 and 48 hpf
323 were collected or were rinsed in filtered seawater and allowed to develop until 72 hpf to observe
324 phenotype. For RA treatments, a final concentration of 10^{-6} M was used. Embryos were
325 collected at the developmental stages of 30, 36, 42 and 48 hpf. All the treatments were
326 performed in biological triplicates.
327 For rescue experiments, embryos at 24 hpf were treated simultaneously with a combination of
328 100 µM TRIM and 25 µM DEAB, or 100 µM TRIM and 10^{-6} M BMS009. At 30 hpf they were
329 rinsed in filtered seawater and allowed to develop until 72 hpf stage when the phenotype was
330 observed. The experiment was performed in biological duplicates.
331 Control and TRIM-treated larvae at 72 hpf were stained with DAPI. A high-resolution Z-stack
332 was acquired using a Zeiss confocal microscopy LSM 800, and a medium speed fast interactive
333 deconvolution was applied. For the digital sections, Imaris 9.3.1 software was used.
334
335 **RNA-seq analysis**

Total RNA was extracted from embryos using the RNeasy Plus Mini Kit (QIAGEN) after sample homogenization using the TissueLyser (QIAGEN). The RNA integrity number (RIN) was assessed by using TapeStatio4200 while RNA concentration and purity were estimated using a Nanodrop spectrophotometer. Indexed libraries were prepared from 1 ug/ea purified RNA with TruSeq Stranded Total RNA Library Prep Kit. Libraries were quantified using the Agilent 2100 Bioanalyzer (Agilent Technologies) and pooled so that each index-tagged sample was present in equimolar amounts, with a final concentration of 2 nM. The pooled samples at a final concentration of 10 pM were subjected to cluster generation and sequencing using an Illumina NextSeq500 System in a 1x75 single read format (30 millions of reads). The raw sequence files generated (fastq files) underwent quality control analysis using FastQC. Transcriptome sequences were deposited in the NCBI Sequence Read Archive (SRA) database with the accession number: PRJNA630453.

Reads were mapped on the *B. lanceolatum* transcriptome (Oulion et al., 2012) using the aligner Bowtie2 with default parameters (Langmead and Salzberg, 2012). The read counts were obtained using IdxStats (Li et al., 2009; Cock et al., 2013) and the differential expression analysis between treated and wild-type embryos was performed using the R package DESeq2 (Love et al., 2014). Mapping and read counting were performed on the Roscoff ABiMS galaxy platform.

Phylogenetic analysis

Phylogenetic analysis was necessary to establish the orthology relationships of the RA synthesis genes differentially expressed in our experiments. Protein alignments were generated with ClustalX program using the sequence database reported in Handberg-Thorsager *et al.* (Handberg-Thorsager et al., 2018) . Phylogenetic trees were based on

maximum-likelihood inferences calculated with PhyML v3.0 (Guindon et al., 2010) (Figure supplement 2).

Computational prediction of DR-type RAREs in *NosA* and *NosB* genomic loci

We selected open chromatin genomic regions in the vicinity of *Nos* genes by choosing regions corresponding to ATAC-seq peaks (8, 15, 36, 60 hpf) overlapping with ChiP-seq signals for the H3K4me3 mark at the same developmental times. The prediction of putative Direct Repeats (DR) binding sites in the genomic loci of *NosA* and *NosB* was assessed by NHR-SCAN tool (Sandelin and Wasserman, 2005), using the following parameter: 0,01 combined probability of entering match states.

Gene expression analysis by whole-mount *in situ* hybridization

Hox1, *Hox3*, *Mei*s, *Cyp26.1*, *Cyp26.2*, *Cyp26.3* were cloned in pGEM-T vector (Promega) using primers listed in Supplementary table 1. Antisense riboprobes were synthesized and *in situ* hybridizations were performed as previously described (Annona et al., 2017). Embryos were mounted in 80% glycerol in PBS, and photographed using an Axio Imager.Z2.

Gene expression analysis by qRT-PCR

Total RNA was extracted from embryos at different developmental stages: 30, 36, 42 and 48 hpf (Figure 1A), using the RNeasy Plus Mini Kit (QIAGEN). 350-1000 ng of total RNA were retrotranscribed in cDNA which was used undiluted (only for *Nos* genes) or diluted 1:10 for the quantitative PCR. Each qPCR reaction contained a final concentration of 0.7 µM of each primer and Fast SYBR Green Master mix with ROX (Applied Biosystems) in 10 µl total volume. PCR reactions were run in a ViiA™ 7 Real-Time PCR System (Applied Biosystems). The cycling

conditions were: 95°C for 20 s, 40 cycles with 95°C for 1 s, 60°C for 20 s, 95°C for 15 s, 60°C 1 min, followed by a dissociation curve analysis using a gradient from 60°C to 95°C with a continuous detection at 0.015°C/sec increment for 15 min. The results were analyzed using the ViiA™-7 Software and exported into Microsoft Excel for further analysis. Each sample was processed in biological triplicates. Ribosomal protein L32 (*Rpl32*), expressed at a constant level during development, was used as a reference gene for the normalization of each gene expression level (Annona et al., 2017). Primers used are listed in Supplementary table 1. For the statistical analysis, we used the GraphPad Prism software employing the T-test. Statistical significance cut off criteria was set at $p<0.05$.

Acknowledgments

The authors thank Rebecca Adikes and Hannah Rosenblatt, course assistants at the MBL Embryology Course 2019 in Woods Hole (USA), for their help with imaging. We are also grateful to Enrico D'Aniello and Ricard Albalat for their critical reading of the manuscript. We are grateful to the Institut Français de Bioinformatique and the Roscoff Bioinformatics platform ABiMS for providing computing and storage resources for the RNA-seq analysis. We thank the BIO2MAR platform for giving us access to analytical material.

SD and FC acknowledge the Assemble Plus Project (contract numbers BA010618 and 360BA0619) and The Company of Biologists (grant number: DEVTF-170211; Sponsoring Journal: Development) for supporting research visits to the Observatoire Océanologique of Banyuls-sur-Mer (France). FC was supported by an OU-SZN PhD fellowship. SB is supported by the Institut Universitaire de France (IUF). HE is supported by the Centre national de la recherche scientifique and Agence Nationale de la Recherche (ANR) grants no. ANR-16-CE12-0008-01 and ANR-19-CE13-0011.

References

Abe M, Maeda T, Wakisaka S. 2008. Retinoic acid affects craniofacial patterning by changing Fgf8 expression in the pharyngeal ectoderm. *Dev Growth Differ* **50**:717–729. doi:10.1111/j.1440-169X.2008.01069.x

Achan V, Tran CTL, Arrigoni F, Whitley GSJ, Leiper JM, Vallance P. 2002. all- trans -Retinoic Acid Increases Nitric Oxide Synthesis by Endothelial Cells. *Circ Res* **90**:764–769. doi:10.1161/01.RES.0000014450.40853.2B

Albalat R, Brunet F, Laudet V, Schubert M. 2011. Evolution of Retinoid and Steroid Signaling: Vertebrate Diversification from an Amphioxus Perspective. *Genome Biol Evol* **3**:985–1005. doi:10.1093/gbe/evr084

Annona G, Caccavale F, Pascual-Anaya J, Kuratani S, De Luca P, Palumbo A, D'Aniello S. 2017. Nitric Oxide regulates mouth development in amphioxus. *Sci Rep* **7**:8432. doi:10.1038/s41598-017-08157-w

Behairi N, Belkhelfa M, Mesbah-Amroun H, Rafa H, Belarbi S, Tazir M, Touil-Boukoffa C. 2015. All-*trans*-Retinoic Acid Modulates Nitric Oxide and Interleukin-17A Production by Peripheral Blood Mononuclear Cells from Patients with Alzheimer's Disease. *Neuroimmunomodulation* **22**:385–393. doi:10.1159/000435885

Bertrand S, Aldea D, Oulion S, Subirana L, de Lera AR, Somorjai I, Escriva H. 2015. Evolution of the Role of RA and FGF Signals in the Control of Somitogenesis in Chordates. *PLoS One* **10**. doi:10.1371/journal.pone.0136587

Bogdan C. 2001. Nitric oxide and the regulation of gene expression. *Trends Cell Biol* **11**:66–75. doi:10.1016/S0962-8924(00)01900-0

Cañestro C, Albalat R, Hjelmqvist L, Godoy L, Jörnvall H, Gonzàlez-Duarte R. 2002. Ascidian and Amphioxus Adh Genes Correlate Functional and Molecular Features of the ADH Family Expansion During Vertebrate Evolution. *J Mol Evol* **54**:81–89. doi:10.1007/s00239-001-0020-2

Cañestro C, Postlethwait JH, Gonzalez-Duarte R, Albalat R. 2006. Is retinoic acid genetic machinery a chordate innovation? *Evol Dev* **8**:394–406. doi:10.1111/j.1525-142X.2006.00113.x

Carvalho JE, Lahaye F, Croce JC, Schubert M. 2017a. CYP26 function is required for the tissue-specific modulation of retinoic acid signaling during amphioxus development. *Int J*

Dev Biol **61**:733–747. doi:10.1387/ijdb.170227ms

Carvalho JE, Theodosiou M, Chen J, Chevret P, Alvarez S, De Lera AR, Laudet V, Croce JC, Schubert M. 2017b. Lineage-specific duplication of amphioxus retinoic acid degrading enzymes (CYP26) resulted in sub-functionalization of patterning and homeostatic roles. *BMC Evol Biol* **17**:24. doi:10.1186/s12862-016-0863-1

Castellano I, Ercolesi E, Palumbo A. 2014. Nitric Oxide Affects ERK Signaling through Down-Regulation of MAP Kinase Phosphatase Levels during Larval Development of the Ascidian Ciona intestinalis. *PLoS One* **9**. doi:10.1371/journal.pone.0102907

Chawla B, Swain W, Williams AL, Bohnsack BL. 2018. Retinoic Acid Maintains Function of Neural Crest–Derived Ocular and Craniofacial Structures in Adult Zebrafish. *Investig Opthalmology Vis Sci* **59**:1924–1935. doi:10.1167/iovs.17-22845

Cock PJA, Grüning BA, Paszkiewicz K, Pritchard L. 2013. Galaxy tools and workflows for sequence analysis with applications in molecular plant pathology. *PeerJ* **1**:e167. doi:10.7717/peerj.167

Duester G. 2008. Retinoic Acid Synthesis and Signaling during Early Organogenesis. *Cell* **134**:921–931. doi:10.1016/j.cell.2008.09.002

Escriva H, Holland ND, Gronemeyer H, Laudet V, Holland LZ. 2002. The retinoic acid signaling pathway regulates anterior/posterior patterning in the nerve cord and pharynx of amphioxus, a chordate lacking neural crest. *Development* **129**:2905–16.

Francis-West P, Crespo-Enriquez I. 2016. Vertebrate Embryo: Craniofacial DevelopmentELS. Chichester, UK: John Wiley & Sons, Ltd. pp. 1–15. doi:10.1002/9780470015902.a0026602

Fuentes M, Benito E, Bertrand S, Paris M, Mignardot A, Godoy L, Jimenez-Delgado S, Oliveri D, Candiani S, Hirsinger E, D'Aniello S, Pascual-Anaya J, Maeso I, Pestarino M, Vernier P, Nicolas JF, Schubert M, Laudet V, Geneviere AM, Albalat R, Garcia Fernandez J, Holland ND, Escriva H. 2007. Insights into spawning behavior and development of the European amphioxus (Branchiostoma lanceolatum). *J Exp Zool B Mol Dev Evol* **308**:484–493.

Gallego O, Belyaeva O V., Porté S, Ruiz FX, Stetsenko A V., Shabrova E V., Kostereva N V., Farrés J, Parés X, Kedishvili NY. 2006. Comparative functional analysis of human medium-chain dehydrogenases, short-chain dehydrogenases/reductases and aldo-keto

reductases with retinoids. *Biochem J* **399**:101–109. doi:10.1042/BJ20051988

Guindon S, Dufayard J-F, Lefort V, Anisimova M, Hordijk W, Gascuel O. 2010. New Algorithms and Methods to Estimate Maximum-Likelihood Phylogenies: Assessing the Performance of PhyML 3.0. *Syst Biol* **59**:307–321. doi:10.1093/sysbio/syq010

Handberg-Thorsager M, Gutierrez-Mazariegos J, Arold ST, Kumar Nadendla E, Bertucci PY, Germain P, Tomançak P, Pierzchalski K, Jones JW, Albalat R, Kane MA, Bourguet W, Laudet V, Arendt D, Schubert M. 2018. The ancestral retinoic acid receptor was a low-affinity sensor triggering neuronal differentiation. *Sci Adv* **4**:1–16. doi:10.1126/sciadv.aao1261

Hattori M, Kato Y, Fujihara N. 2002. Retinoic acid suppression of endothelial nitric oxide synthase in porcine oocyte. *Can J Physiol Pharmacol* **80**:777–782. doi:10.1139/y02-099

Haworth KE, Wilson JM, Grevellec A, Cobourne MT, Healy C, Helms JA, Sharpe PT, Tucker AS. 2007. Sonic hedgehog in the pharyngeal endoderm controls arch pattern via regulation of Fgf8 in head ectoderm. *Dev Biol* **303**:244–258. doi:10.1016/j.ydbio.2006.11.009

Jacox L, Sindelka R, Chen J, Rothman A, Dickinson A, Sive H. 2014. The Extreme Anterior Domain Is an Essential Craniofacial Organizer Acting through Kinin-Kallikrein Signaling. *Cell Rep* **8**:596–609. doi:10.1016/j.celrep.2014.06.026

Kong Y, Grimaldi M, Curtin E, Dougherty M, Kaufman C, White RM, Zon LI, Liao EC. 2014. Neural Crest Development and Craniofacial Morphogenesis Is Coordinated by Nitric Oxide and Histone Acetylation. *Chem Biol* **21**:488–501. doi:10.1016/j.chembiol.2014.02.013

Koop D, Chen J, Theodosiou M, Carvalho JE, Alvarez S, de Lera AR, Holland LZ, Schubert M. 2014. Roles of retinoic acid and Tbx1/10 in pharyngeal segmentation: amphioxus and the ancestral chordate condition. *Evodevo* **5**:36. doi:10.1186/2041-9139-5-36

Koop D, Holland ND, Sémon M, Alvarez S, de Lera AR, Laudet V, Holland LZ, Schubert M. 2010. Retinoic acid signaling targets Hox genes during the amphioxus gastrula stage: Insights into early anterior–posterior patterning of the chordate body plan. *Dev Biol* **338**:98–106. doi:10.1016/j.ydbio.2009.11.016

Langmead B, Salzberg SL. 2012. Fast gapped-read alignment with Bowtie 2. *Nat Methods* **9**:357–359. doi:10.1038/nmeth.1923

Lee C-M, Tripathi S, Morgan ET. 2017. Nitric oxide-regulated proteolysis of human CYP2B6 via the ubiquitin-proteasome system. *Free Radic Biol Med* **108**:478–486. doi:10.1016/j.freeradbiomed.2017.04.015

Lee C, Lee B, Arnold SL, Isoherranen N, Morgan ET. 2014. Nitric Oxide and Interleukin-1 β Stimulate the Proteasome-Independent Degradation of the Retinoic Acid Hydroxylase CYP2C22 in Primary Rat Hepatocytes. *J Pharmacol Exp Ther* **348**:141–152. doi:10.1124/jpet.113.209841

Li G, Liu X, Xing C, Zhang H, Shimeld SM, Wang Y. 2017. Cerberus–Nodal–Lefty–Pitx signaling cascade controls left – right asymmetry in amphioxus. *Proc Natl Acad Sci* **114**:3684–3689. doi:10.1073/pnas.1620519114

Li H, Handsaker B, Wysoker A, Fennell T, Ruan J, Homer N, Marth G, Abecasis G, Durbin R. 2009. The Sequence Alignment/Map format and SAMtools. *Bioinformatics* **25**:2078–2079. doi:10.1093/bioinformatics/btp352

Liu Y, Lu X, Xiang F-L, Lu M, Feng Q. 2013. Nitric Oxide Synthase-3 Promotes Embryonic Development of Atrioventricular Valves. *PLoS One* **8**:e77611. doi:10.1371/journal.pone.0077611

Love MI, Huber W, Anders S. 2014. Moderated estimation of fold change and dispersion for RNA-seq data with DESeq2. *Genome Biol* **15**:550. doi:10.1186/s13059-014-0550-8

Marlétaz F, Firbas PN, Maeso I, Tena JJ, Bogdanovic O, Perry M, Wyatt CDR, de la Calle-Mustienes E, Bertrand S, Burguera D, Acemel RD, van Heeringen SJ, Naranjo S, Herrera-Ubeda C, Skvortsova K, Jimenez-Gancedo S, Aldea D, Marquez Y, Buono L, Kozmikova I, Permanyer J, Louis A, Albuixech-Crespo B, Le Petillon Y, Leon A, Subirana L, Balwierz PJ, Duckett PE, Farahani E, Aury J-M, Mangenot S, Wincker P, Albalat R, Benito-Gutiérrez È, Cañestro C, Castro F, D'Aniello S, Ferrier DEK, Huang S, Laudet V, Marais GAB, Pontarotti P, Schubert M, Seitz H, Somorjai I, Takahashi T, Mirabeau O, Xu A, Yu J-K, Carninci P, Martinez-Morales JR, Crollius HR, Kozmik Z, Weirauch MT, Garcia-Fernàndez J, Lister R, Lenhard B, Holland PWH, Escriva H, Gómez-Skarmeta JL, Irimia M. 2018. Amphioxus functional genomics and the origins of vertebrate gene regulation. *Nature* **564**:64–70. doi:10.1038/s41586-018-0734-6

Minoux M, Rijli FM. 2010. Molecular mechanisms of cranial neural crest cell migration and patterning in craniofacial development. *Development* **137**:2605–2621.

533 doi:10.1242/dev.040048
534 Moon K-Y. 2019. Upregulation of Nitric Oxide Synthase Activity by All- trans Retinoic Acid and
535 13- cis Retinoic Acid in Human Malignant Keratinocytes. *Biomed Sci Lett* **25**:196–200.
536 doi:10.15616/BSL.2019.25.2.196
537 Nott A, Watson PM, Robinson JD, Crepaldi L, Riccio A. 2008. S-nitrosylation of histone
538 deacetylase 2 induces chromatin remodelling in neurons. *Nature* **455**:411–415.
539 doi:10.1038/nature07238
540 Oulion S, Bertrand S, Belgacem MR, Le Petillon Y, Escriva H. 2012. Sequencing and Analysis
541 of the Mediterranean Amphioxus (Branchiostoma lanceolatum) Transcriptome. *PLoS One*
542 **7**:e36554. doi:10.1371/journal.pone.0036554
543 Sandelin A, Wasserman WW. 2005. Prediction of Nuclear Hormone Receptor Response
544 Elements. *Mol Endocrinol* **19**:595–606. doi:10.1210/me.2004-0101
545 Schubert M, Holland ND, Laudet V, Holland LZ. 2006. A retinoic acid-Hox hierarchy controls
546 both anterior/posterior patterning and neuronal specification in the developing central
547 nervous system of the cephalochordate amphioxus. *Dev Biol* **296**:190–202.
548 doi:10.1016/j.ydbio.2006.04.457
549 Schubert M, Yu J-K, Holland ND, Escriva H, Laudet V, Holland LZ. 2005. Retinoic acid
550 signaling acts via Hox1 to establish the posterior limit of the pharynx in the chordate
551 amphioxus. *Development* **132**:61–73. doi:10.1242/dev.01554
552 Sha Y, Marshall HE. 2012. S-nitrosylation in the regulation of gene transcription. *Biochim*
553 *Biophys Acta - Gen Subj* **1820**:701–711. doi:10.1016/j.bbagen.2011.05.008
554 Sirsjö A, Gidlöf AC, Olsson A, Törmä H, Ares M, Kleinert H, Förstermann U, Hansson GK.
555 2000. Retinoic Acid Inhibits Nitric Oxide Synthase-2 Expression through the Retinoic Acid
556 Receptor-α. *Biochem Biophys Res Commun* **270**:846–851. doi:10.1006/bbrc.2000.2535
557 Soukup V, Yong L, Lu T-M, Huang S-W, Kozmik Z, Yu J-K. 2015. The Nodal signaling
558 pathway controls left-right asymmetric development in amphioxus. *Evodevo* **6**:5.
559 doi:10.1186/2041-9139-6-5
560 Wang H, Holland PWH, Takahashi T. 2019. Gene profiling of head mesoderm in early
561 zebrafish development: insights into the evolution of cranial mesoderm. *Evodevo* **10**:14.
562 doi:10.1186/s13227-019-0128-3
563

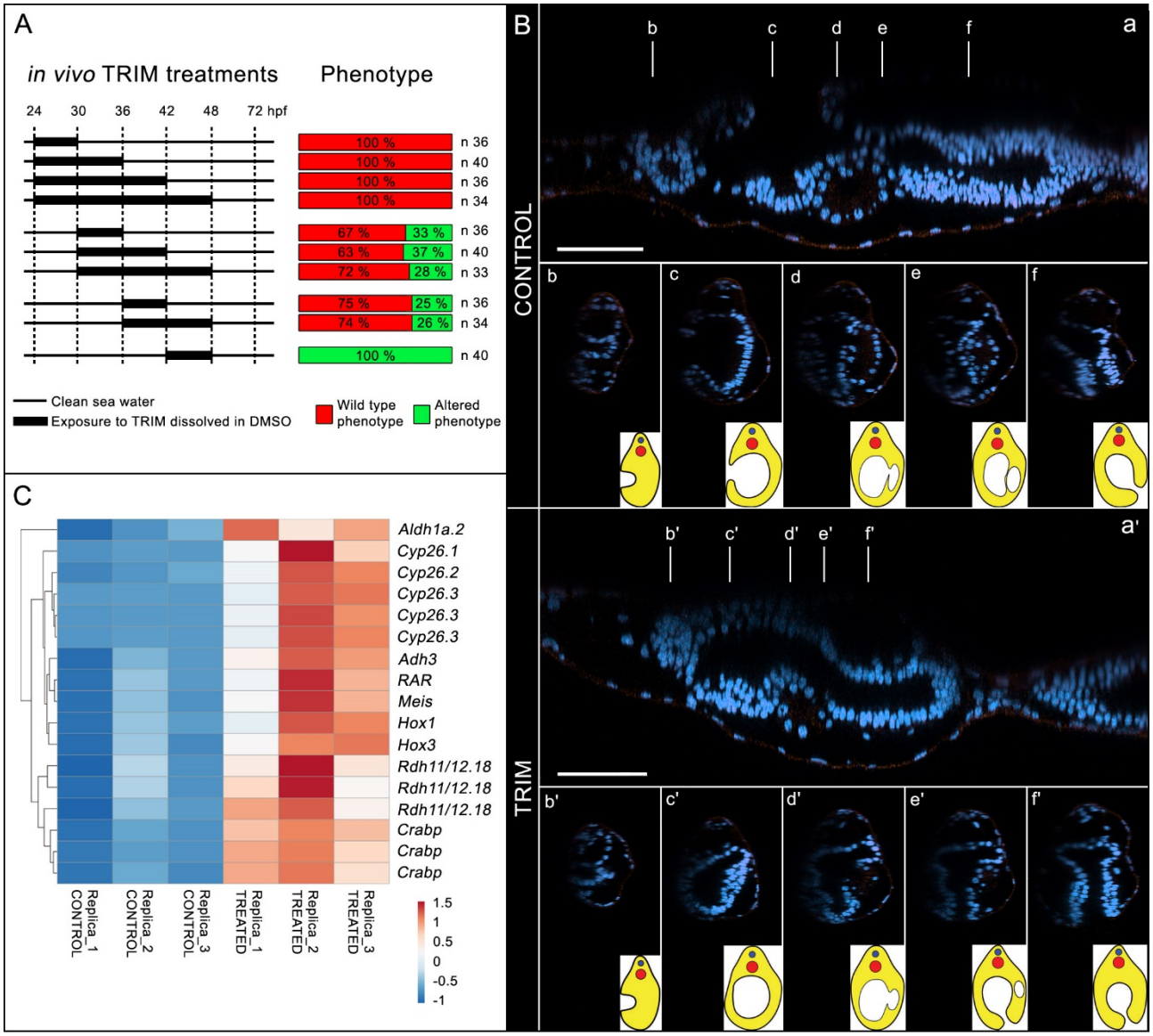

Figure 1. Phenotypic characterization of in vivo TRIM treatment during early amphioxus embryogenesis. A) Schematic representation of time intervals during which embryos were grown in presence of TRIM and the obtained resulting phenotype. B) Digital sections of control and TRIM-treated larvae after DAPI staining showing alteration in pharyngeal region. Anterior to the left. C) Gene expression heatmap of differential transcriptomic analysis (control versus TRIM).

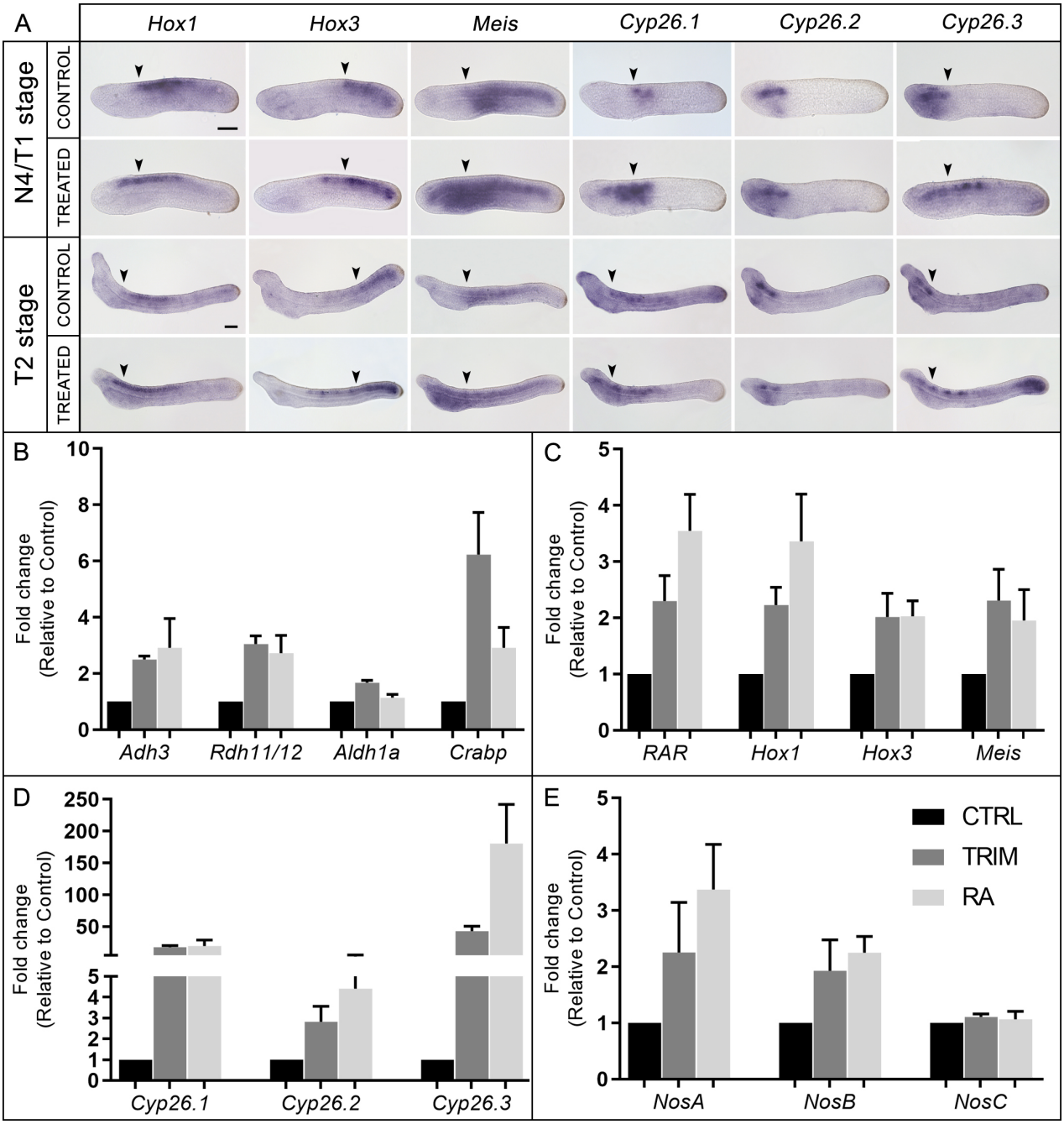

Figure 2. Analysis of gene expression. A) Gene expression pattern by *in situ* hybridization of *Hox1*, *Hox3*, *Meis*, *Cyp26.1*, *Cyp26.2* and *Cyp26.3* after the inhibition of NO production and in controls in 30 hpf (N4/T1 stage) and 42 hpf (T2) embryos. The anterior (*Hox1*, *Hox3*, *Meis*, *Cyp26.1*) and posterior (*Cyp26.3*) limits of gene expression territories in a wild type embryo are indicated with arrowheads in both control and TRIM-treated conditions showing the posteriorization (or anteriorization for *Cyp26.*3) of gene expression in treated embryos. Embryos orientation: anterior to the left, dorsal to the top. Scale bars: N4/T1 stage: 50µM; T2 stage: 50µM. **B-E)** Histograms of qRT-PCR experiment results show expression level changes, after 6 hours of pharmacological TRIM or RA treatments, of: **B)** genes encoding enzymes for RA synthesis: *Adh3*, *Rdh11/12.18*, *Aldh1a.2* and binding protein for storage: *Crabp*; **C)** genes known as direct targets of RA: *Hox1*, *Hox3*, *Meis*, *RAR*; **D)** genes encoding RA degradation enzymes: *Cyp26.1*, *Cyp26.2*, *Cyp26.3*; **E)** *Nos* genes: *NosA*, *NosB*, *NosC*. The gene expression analyses were performed by qRT-PCR on 30 hpf embryos (N4) RNA samples. The statistical analysis showed a pvalue <0,05 for all the data, except for *NosA* after TRIM in **(E)** that show a pvalue = 0,07.

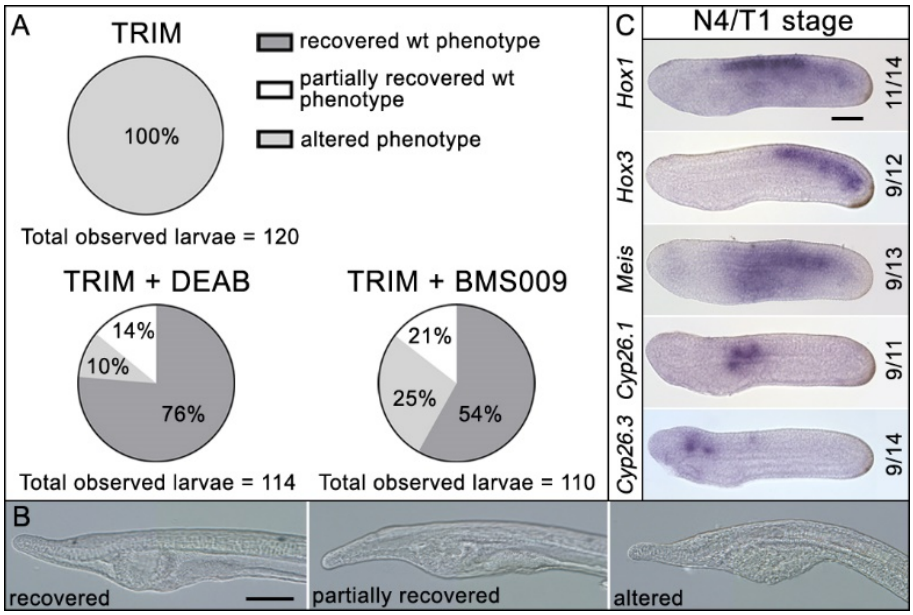

Figure 3. Phenotypic rescue effect of DEAB and BMS009 on TRIM-treated embryos. A) Pie charts of the phenotypes observed after TRIM treatment and the combinatorial pharmacological treatments TRIM (100 µM) + DEAB (25 µM) and TRIM (100 µM) + BMS009 (10-6 M). The percentages of each observed phenotype are reported in the respective portions of the graphs. For each treatment, the total number of observed larvae is indicated below the chart. B) Pictures of the pharyngeal region of larvae presenting the three different classes of phenotype observed in the rescue experiments: recovered wild type phenotype, partially recovered wild type phenotype, altered phenotype. C) Gene expression pattern analyses by *in situ* hybridization of *Hox1*, *Hox3*, Meis, *Cyp26.1*, and *Cyp26.3* after rescue assay with DEAB show the restoration of wild-type gene expression territories of the analyzed genes. *Cyp26.2* expression was not assayed because its localization in the embryo does not change after TRIM treatment. The numbers indicate the ratio between embryos showing a restored expression pattern and the total number of embryos analyzed. Embryos orientation: anterior to the left, dorsal to the top. Scale bar: 50 µM.

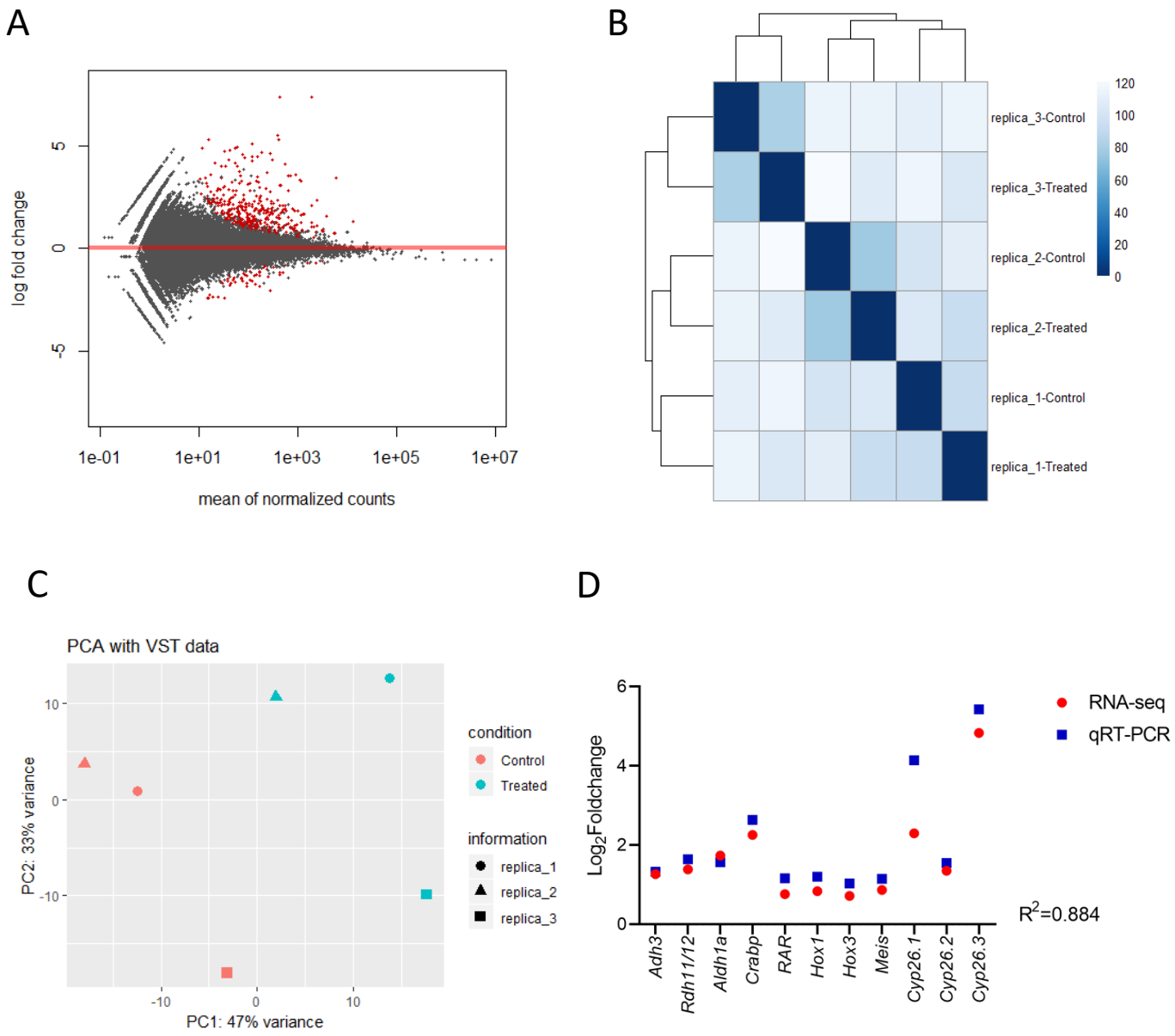

Figure supplement 1. Quality of RNA-seq data. A) MA plot, red dots plotted represent genes with an adjusted *p* value < 0,1 (treated vs control). B) Heatmap of sample-to-sample distances, strains are clustered by replicas (3 controls and 3 treated); C. Principal component analysis (PCA) plot. Sample classes are highlighted in different colors: control in red and treated in blue. D) Gene expression correlation between RT-qPCR and RNA-seq data for the following selected genes: Adh3, Rdh11/12.18, Aldh1a.2, Crabp, RAR, Hox1, Hox3, Meis, Cyp26.1, Cyp26.2 and Cyp26.3.
Blu squares indicate Log2 of relative foldchanges obtained from RT-qPCR analysis of TRIM-treated versus untreated samples. Red circles indicate Log2 of relative foldchanges obtained from RNAseq analysis of TRIM-treated versus untreated samples. The Pearson correlation Coefficient (R2) is indicated.

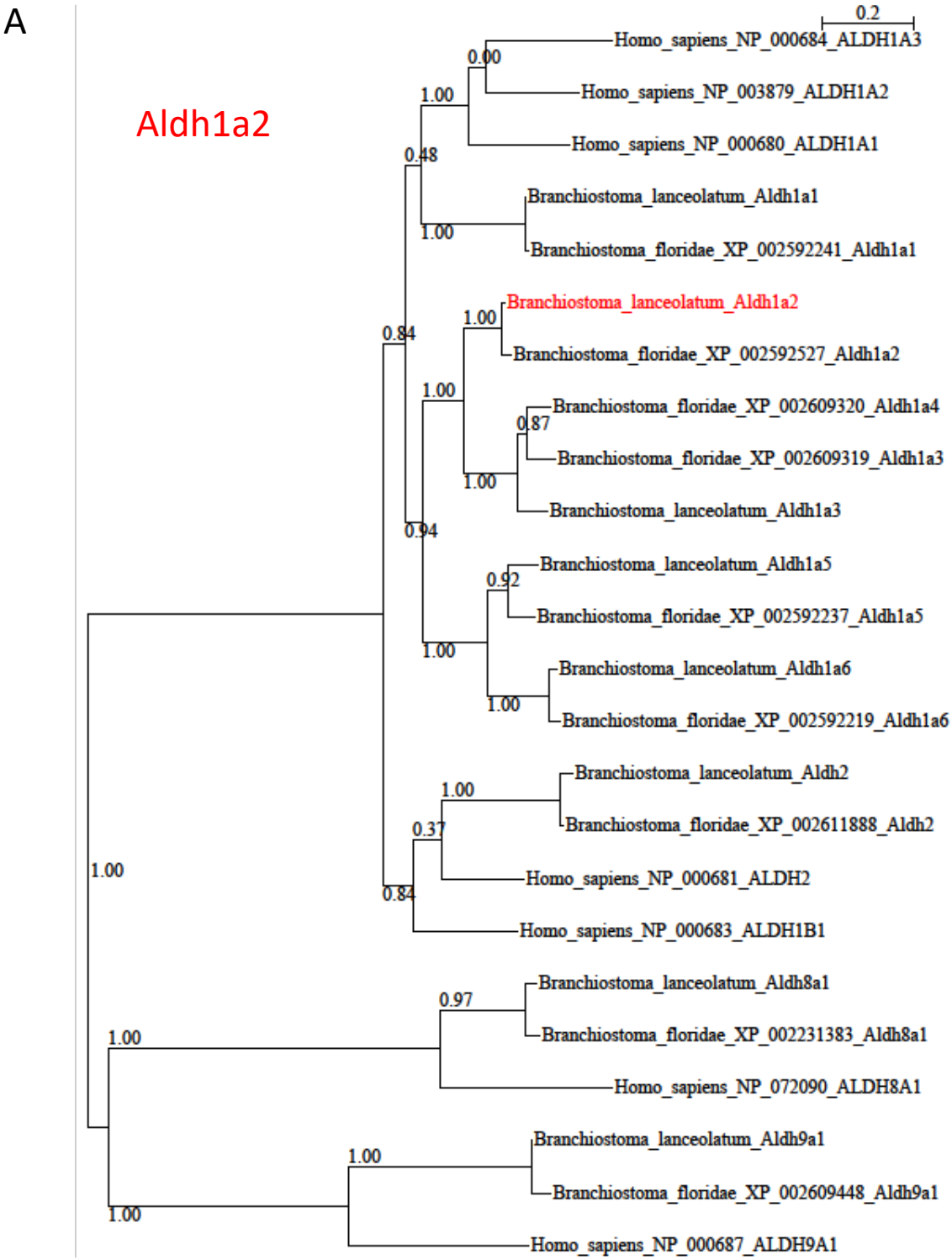

Figure supplement 2. Phylogenetic analysis of RA pathway genes resulted upregulated in the differential WT versus TRIM transcriptome. The analysis allowed the identification of *Branchiostoma lanceolatum* homologs (indicated in red in the trees) for (A) Aldh1a2 (ContigAmph4820) and (B) Rdh11/12.18 (ContigAmph8913/ContigAmph35515/ContigAmph81467). Trees were calculated using Maximum Likelihood (ML) method, and bootstrap supports are given at each node. The GenBank accession number is indicated for each protein sequence used.

Figure supplement 2B

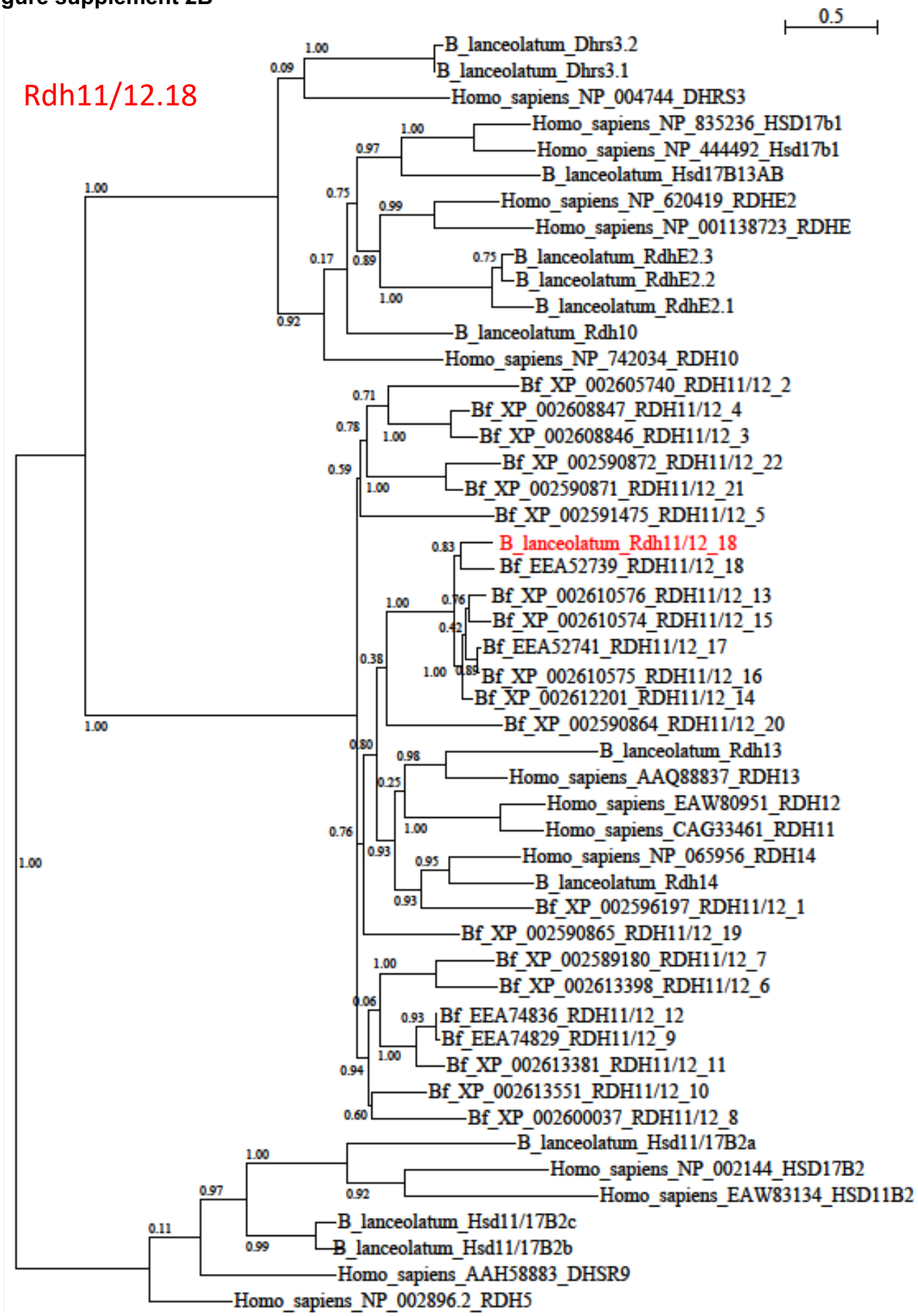

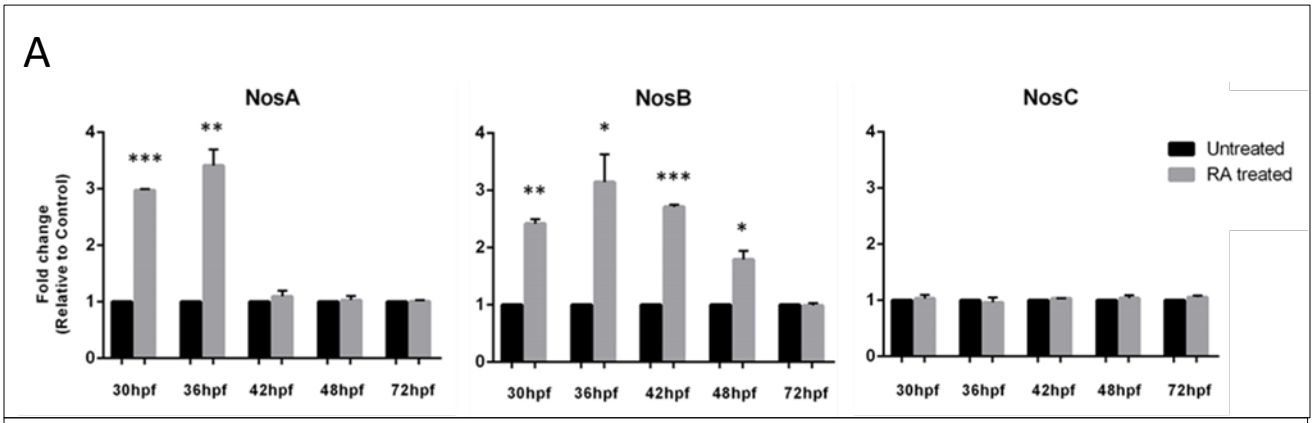

B

NosA

Scaffold 253 - coordinates of surveyed sequences: 298,591 - 351,050 (52,460 bp)

NosA gene coordinates: 299,892 - 330,854 (30,963 bp) (minus)

DR type	Sequence	Coordinates
DR1	TGCCCTGTGCCCA	313,686 - 313,698
DR1	GGTTAGTGGTCAA	315,338 - 315,350
DR3	TGGTCAATTAGTACA	313,997 - 314,011
DR3	TGGTCAATTAGTACA	327,253 - 327,267
DR3	GTGTCAATAAGTTCA	332,729 - 332,743
DR5	TGAACTTCAGATGAACT	332,905 - 332,921

NosB

Scaffold 25 - coordinates of surveyed sequences: 516,054 - 541,160 (25,107 bp)

NosB gene coordinates: 519,314 - 535,503 (16,190 bp) (plus)

DR type	Sequence	Coordinates
DR3	AGCTCAGCCAGGTCA	519,296 - 519,310

Figure supplement 3. A) *Nos* genes expression pattern by RT-qPCR after RA treatment during amphioxus development. Five developmental time points were assayed from 30 to 72 hours post-fertilization. * = pvalue<0,05; **= pvalue<0,005; ***= pvalue<0,001. **B)** *In silico* prediction analysis of RARE elements in genomic loci of Branchiostoma lanceolatum NosA and NosB. The analysis was limited to neighboring genes on both sides of each Nos gene. Direct Repeat 1 (DR1) are shown in blue, DR3 in green and DR5 in red. Sequence and coordinates of each putative DR are indicated.

Probes for *in situ* hybridization		
Genes	**Forward and reverse primer**	**Product length (bp)**
Hox1	5'- GAGCAAATGGACACGGCAAG -3' 5'- CTTCGACGGGCTATCTTCAC -3'	855 bp
Hox3	5'- GAGGTGGTGGCAGCTATGG -3' 5'- CGCAGTAGTTCATATTGACCAC -3'	1077 bp
Meis	5'- CAGTCGCCACGTCTATGTACG -3' 5'- CTGGACTATCCTGCGCCTC -3'	983 bp
Cyp26.1	5'- GCTGGTACTGGTGCTGTGGAG -3' 5'- ACATCACGCGCCGCTAACAC -3'	759 bp
Cyp26.2	5'- CTGCTGCTGTCCTGGAAGCTG -3' 5'- GTCTCCACTGTCTCCTCCCTG -3'	720 bp
Cyp26.3	5'- CAGACTTCTCCCGTAAGCGAC -3' 5'- CCCCAACAGGTGGACTTAGC -3'	891 bp
Real time RT-PCR primers		
Genes	**Forward and reverse primer**	**Product length (bp)**
Adh3	5'- GTCCCACAGTGCAAGGAGTG -3' 5'- CCACCGTGTACTCGCTGAAG -3'	175 bp
Rdh11/12_18	5'- CAGCAGGAGGGAAGTGTGAG -3' 5'- GGACGCAAGGTCAAGTTTCTG -3'	227 bp
Aldh1a_2	5'- GTAAGATCATCCAGGCAGCAG -3' 5'- CGTCGTAGACAGATTCCTCCAC -3'	201 bp
Crabp	5'- GTCAGCTTCAAGATCGGAGAG -3' 5'- CTTCATCACCAGGTACATCCG -3'	171 bp
RAR	5'- GTCGTCTGGCTACCACTACGG -3' 5'- ACCTGCAGAACTGGCATCTG -3'	152 bp
Hox1	5'- GGATACATGCACCACCATACG -3' 5'- GTCCGTCCGTTGTTGGGTCCG -3'	176 bp
Hox3	5'- CCGACAACAACCACAGCAG -3' 5'- CACAGGTAGCGGTTGAAGTGG -3'	256 bp
Meis	5'- CAGTCGCCACGTCTATGTACG -3' 5'- GAAAGAGTGGATGCCCGTAG -3'	198 bp
Cyp26.1	5'- GCTGGTACTGGTGCTGTGGAG -3' 5'- CGTGGAGAATCTTGCGCAC -3'	248 bp
Cyp26.2	5'- CAGGGAGGAGACAGTGGAGAC -3' 5'- CTTCTCCAGGTCCTCATGCAC -3'	210 bp
Cyp26.3	5'- CAGGAAGTTGCGGCATATCTTG -3' 5'- GTCGCTTACGGGAGAAGTCTG -3'	190 bp
NosA	5'- AGTACAGTCATCTCCAGAAC -3' 5'- TCTTGCAAGCGCTTCTATCTG -3'	221 bp
NosB	5'- AGTTTACTCCCGGCGATCA -3' 5'- AGAACATGGCGGCAAACGC -3'	191 bp
NosC	5'- CAGGATTCTGCGCGTTTGC -3' 5'- GGAGCTAGCCTCGCTCATG -3'	197 bp
Rpl32	5'- GGCTTCAAGAAATTCCTCGTC -3' 5'- GATGAGTTTCCTCTTGCGCGA -3'	117 bp

Supplementary table 1. Oligonucleotides used to amplify probes for *in situ* hybridization experiments and for Real time RT-PCR analyses.